Strain-induced first-order orbital flip transition and coexistence of charge-orbital ordered phases in $Pr_{0.5}Ca_{0.5}MnO_3$

P. R. Sagdeo, N. P. Lalla, and A. V. Narlikar
UGC-DAE Consortium for Scientific Research, University Campus, Khandwa Road, Indore 452017, India

D. Prabhakaran and A. T. Boothroyd
Clarendon Laboratory, Department of Physics, University of Oxford, Parks Road, Oxford OX1 3PU, United Kingdom
(Received 18 April 2008; revised manuscript received 20 August 2008; published 7 November 2008)

Low-temperature transmission electron microscopy and x-ray diffraction (XRD) studies have been carried out on pellet and powder samples of $Pr_{0.5}Ca_{0.5}MnO_3$. These studies have revealed appearance of a different type of charge-orbital ordered (COO) phase, resulting due to flipping of e_g orbitals from $d_{3x^2-r^2}/d_{3y^2-r^2}$ to $d_{3x^2-r^2}/d_{3z^2-r^2}$ configuration. This orbital flip results in a changeover of the COO superlattice-ordering vector from (1/2,0,0) to (1/4,1/2,1/4) in the *Pnma* phase. This COO phase coexists with the conventional COO phase. Low-temperature XRD studies show that the COO phase appears only in pellet sample and not in the corresponding powder sample. The powder sample shows only conventional COO phase. Volume fractions of conventional and the other type COO phases in pellet sample of $Pr_{0.5}Ca_{0.5}MnO_3$ is estimated to be ~55% and 45%, respectively. The occurrence of orbital flip has been attributed to local strain building up in the pellet sample. The strain builds up during cooling because manganite has anisotropic thermal expansion coefficients.

DOI: 10.1103/PhysRevB.78.174106 PACS number(s): 75.47.Lx, 68.37.Lp, 87.15.Zg, 83.10.Tv

I. INTRODUCTION

The manganites show nanometer to micrometer sized phase coexistence of ferromagnetic and antiferromagnetic states,[1] metallic and insulating states,[2] and charge-orbital ordered (COO) phase with a monoclinic phase without COO.[3,4] The electronic and magnetic phase coexistence in manganites is closely related with the three attributes of the e_g electrons, namely, the charge, spin, and the orbital degrees of freedom.[5] e_g electrons are scattered not only by strong electron correlation effect but also by strong electron-lattice coupling arising due to Jahn-Teller (JT) effect. The JT effect is manifested in the form of local or collective distortion of the O_6 octahedra. Since e_g electrons are invariably associated with the lattice distortion, the lattice degrees of freedom are critical to the physical properties of manganites. Despite the theories based on *A*-site chemical disorder[6–9] and composite electronic wave functions,[10] theory incorporating primarily the structural aspects, such as elastic energy landscapes (strain field), do predict[11] both nanometer and micrometer sized coexisting phases in manganites. The lattice degrees of freedom is also important for charge-density wave picture of COO, which slides on application of even weak electric field.[12] It is to be noted that most of the micron size phase coexistence has been found in samples prepared out of bulk, either ceramics or single crystals,[1,2] in which strain field are expected to be present as a result of their processing. Only recently a clear correlation between intrinsic strain and the coexistence of COO and without COO (monoclinic) phases has been reported.[3,11] The phase coexistence has been probed through variety of techniques, such as Lorentz transmission electron microscopy (TEM),[1] electron spectroscopy for chemical analysis (ESCA) microscopy,[2] x-ray diffraction (XRD),[3] and polarized optical microscopy.[13] Looking into theoretical expectations[11,14] and experimental observations,[3] the structural, electrical, and magnetic properties may have appreciable difference in pellet and powder versions of the manganite sample. Such studies are important from the point of view that most of the basic physical property studies on manganites are being carried out on well sintered polycrystalline pellet samples but its results are very frequently being correlated with the phase characterization results, obtained using powder sample.

The effect of strain may not be identical for all type of manganites because they have different band filling and bandwidths. For example the $Pr_{0.5}Ca_{0.5}MnO_3$ (PCMO) is supposed to be very robust charge-orbital ordered phase[15] and hence the effect of strain may not be identical to that of the $La_{-x}Ca_xMnO_3$.[3] Recently all together a different first-order phase transition giving rise to an abrupt change in the electric-field gradient has been reported[16] in polycrystalline pellet of PCMO between COO transition (T_{co}) and Néel temperatures. The origin of this unexpected transition has not been discussed.[16] It may be a manifestation of some lattice degrees of freedom.

With above in mind, we have carried out low-temperature TEM and XRD studies on pellet and powder samples of PCMO. PCMO is an otherwise well studied manganite.[17–19] We have observed a phase transition of conventional[20,21] COO phase with ordering vector [1/2,0,0] into a different type of COO phase: here after termed as COO1 and COO2. This has been attributed to strain induced first-order flip transition of ordered e_g orbitals in COO1 phase. An experimental observation giving evidence of flipping of ordered e_g orbitals, resulting in a different COO phase, is yet not reported.

II. EXPERIMENTAL

The sample of $Pr_{0.5}Ca_{0.5}MnO_3$ was prepared following the conventional solid-state reaction route.[22] The as-prepared pellet of $Pr_{0.5}Ca_{0.5}MnO_3$ was cut across the thickness[3] in two parts. XRD measurements at room temperature (RT) and low

temperature, down to 90 K, were done on the cut surface of one of the pieces of the cut pellet and also on the powder. The powder was obtained by 3–4 min gentle grinding of the other half of the pellet using agate mortar pestle. The grinding was intended just to separate each single-crystal grains. Sample for TEM analysis was prepared out of the inner bulk of the pellet using twin Ar-ion guns operating at 3 kV and set at ~3°. TEM was carried out in imaging and diffraction modes at various temperatures between 96 and 300 K using a LN_2 based double tilt holder (Gatan model 636MA). We explored about twenty randomly selected thin grains in the $Pr_{0.5}Ca_{0.5}MnO_3$ sample at 96 K and recorded selected area electron diffraction (SAD), convergent beam electron-diffraction (CBED) patterns, and corresponding electron micrographs from these grains. Out of these twenty grains, we could encounter only five grains (25%), which showed phase coexistence as discussed below. The locations of these five grains were randomly distributed. In the following we present a gist of the extensive electron diffraction and imaging studies on these grains.

III. RESULTS AND DISCUSSIONS

Figure 1(a) shows the electron micrograph and Figs. 1(b)–1(e) show [010] zone SAD patterns taken from domain D4 at RT: 376, 220, and 96 K respectively. Weak but well-defined incommensurate superlattice spots can be clearly seen in Fig. 1(b). In the present investigation these superlattice spots were observed even at temperatures as high as 376 K. Compare the superlattice spots marked by arrows in Figs. 1(b) and 1(c). Presence of diffuse diffracted intensity arising due to room-temperature incommensurate COO in single-crystal $Pr_{0.5}Ca_{0.5}MnO_3$ was first realized through x-ray diffraction by Shimomura *et al.*[19] This has been attributed to the presence of short-range COO correlation in $Pr_{0.5}Ca_{0.5}MnO_3$ (Ref. 19) at RT. Our TEM observation indicates that in $Pr_{0.5}Ca_{0.5}MnO_3$ this short-range COO correlation persists even at 376 K. We could record even the feeble presence of COO in SAD because electron has several orders higher scattering amplitude (~10^4 times) than that of the x rays. At lower temperatures these weak incommensurate superlattice spots start getting closer and become more intense and sharp [Fig. 1(d)], and finally at ~96 K they merge[19] to each other and give rise to COO1 phase [Fig. 1(e)]. This behavior of COO phase was observed in domains D4 and D5 but the scenario of temperature dependence of [010] zone pattern in domain D2 was found to be completely different. In domain D2, while lowering the temperature, the incommensurate superlattice spots neither became sharper nor got merged to each other, giving rise to COO1 phase with [1/2,0,0] commensurate ordering vector. There was almost no change down to 170 K except for some minor increase in the tilt angle of the superlattice spots about their fundamental spots. But at ~150 K all the COO superlattice spots present in [010] zero-order Laue zone (ZOLZ) pattern corresponding to COO1 phase suddenly disappeared, leaving only the reflections corresponding to *Pnma* phase. The temperature variation in charge-orbital ordering in domain D2 was monitored by recording [010] zone SAD pattern at various temperatures. At each temperature, on which [010] ZOLZs were recorded using SAD, corresponding higher order Laue zone (HOLZ) rings were also recorded using CBED. Disappearance of COO1 superlattice spots in ZOLZ was simultaneously followed by appearance of two extra HOLZ rings in the corresponding CBED pattern. Figures 2(a) and 2(b) show ZOLZ and Figs. 2(c) and 2(d) show CBED patterns taken at 290 and 96 K. As compared to SAD taken at 290 K [in Fig. 2(a)], complete absence of COO superlattice spots can be seen in the SAD taken at 96 K [Fig. 2(b)]. Figure 2(d) shows 96 K CBED with two extra HOLZ rings as compared to 290 K CBED. Appearance of extra HOLZ rings directly indicates the formation of different reciprocal-lattice layers at $[0,N/2,0]$ (N being odd integer) along [010] in the reciprocal lattice of *Pnma* phase. This confirms the transformation

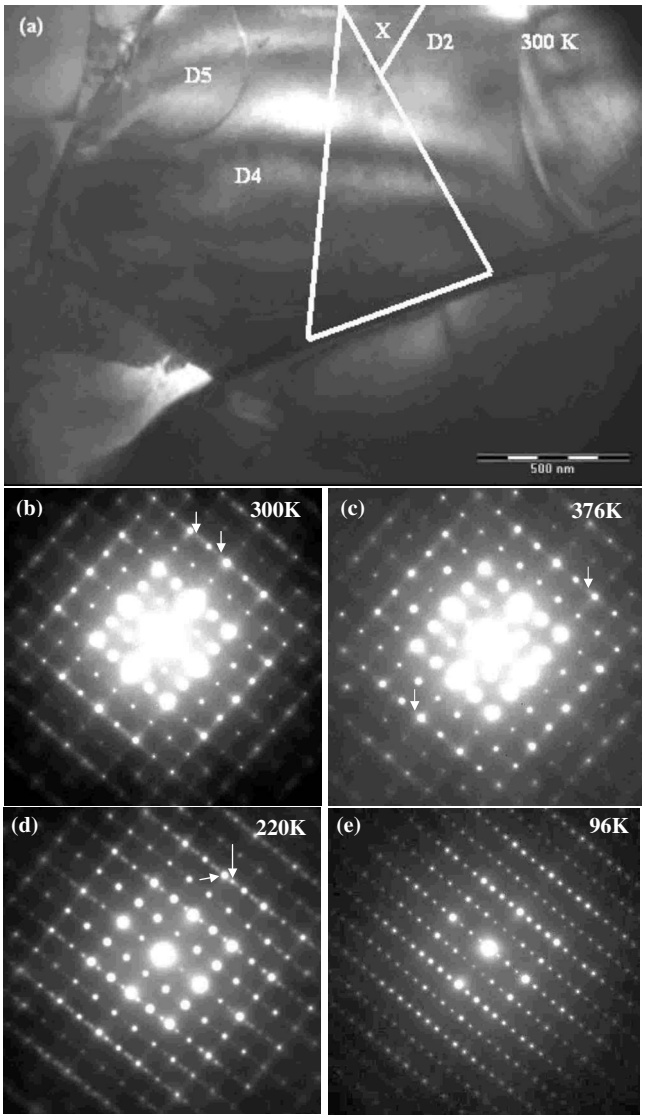

FIG. 1. (a) Electron micrograph showing microstructures of a grain of $Pr_{0.5}Ca_{0.5}MnO_3$ manganite seen along [010] zone. Various domains representing different orientational variants of the manganite can be seen. [(b)–(e)] [010] zone SAD patterns taken from domain D4 at different temperatures. Occurrence of incommensurate to commensurate COO can be seen with decreasing temperature.

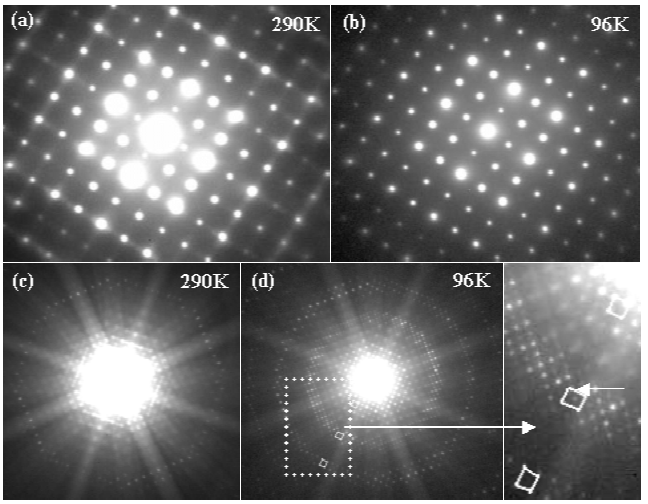

FIG. 2. [(a) and (b)] SADs taken from region X at 290 and 96 K, respectively. (c) and (d) are the corresponding CBED patterns at 290 and 96 K, respectively. Disappearance of COO spots from SAD in (b) and simultaneous occurrence of two extra HOLZ rings in the CBED in (d) can be clearly seen.

of COO1 into a different phase, which has already been termed as COO2. For each reciprocal layer, the unit cells have been indicated [Fig. 2(d)]. It should be noted that as compared to ZOLZ the spot pattern of the formed reciprocal-lattice layer at [0,1/2,0], i.e., the FOLZ in Fig. 2(d), has a spot in its unit-cell center. To monitor possible hysteresis the [010] ZOLZ patterns were recorded at various temperatures during cooling and heating cycles between 290 and 96 K. Figure 3 shows a plot of the ratio of intensities of a superlattice reflection to a fundamental reflection against the temperature at which it was recorded. The fundamental and superlattice reflections used for this purpose are indicated in Fig. 1(d) by short and long arrows, respectively. This plot depicts a well-defined hysteresis in the observed phase transition. The inset of Fig. 3 shows the temperature variation in the tilting of the superlattice spots about the fundamental spot.

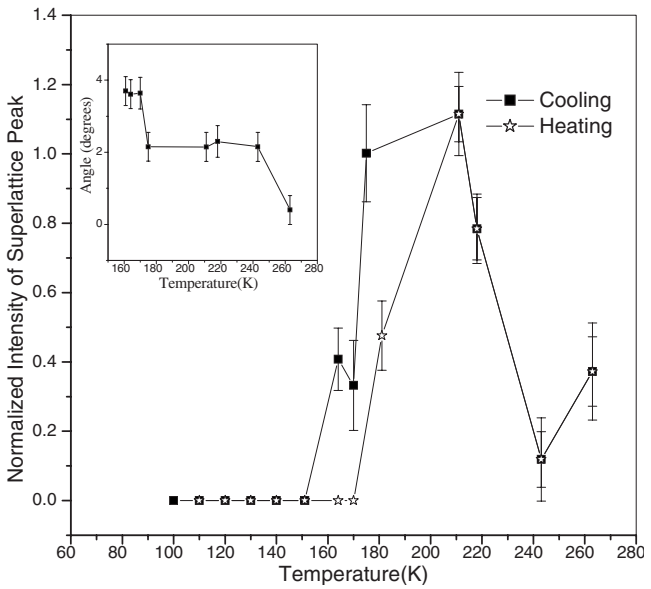

FIG. 3. Hysteresis curve showing the temperature variation in the ratio of intensities of a COO superlattice reflection to the basic reflection from *Pnma* during heating and cooling cycles. The inset shows temperature variation in the tilt angle of the superlattice spots about the fundamental spot.

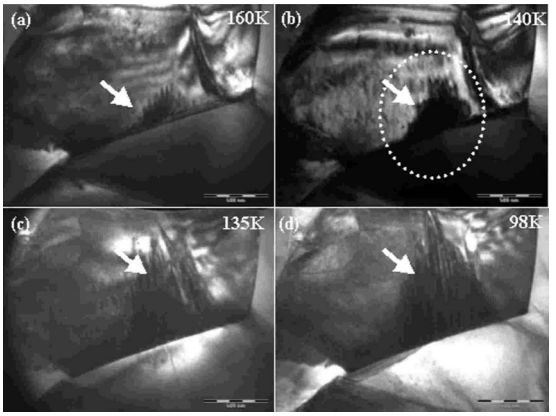

FIG. 4. Electron micrographs taken at different temperatures. It shows the temperature variation in the microstructure of the triangular region showing the COO phase coexistence. The area of the triangular region increases with decreasing temperature. It can be noticed that the triangular patch starts growing from the grain boundary, where presence of strain is most likely.

The microstructural evolution of the grain under observation is shown in Fig. 4. As temperature decreases, a triangular patch starts growing slowly from the grain boundary and diverges at 96 K, separating the two regions. The triangular patch is basically a bunch of twins of COO1 and COO2 phases. It is only at the vertex of the triangular region that the COO1 and COO2 (region X of D4) were found to be large enough, and recording a clean SAD pattern became possible. The SAD taken from the common region is shown in Fig. 5(a). An enlarged view of a part of the SAD is shown in Fig. 5(b). It should be noted that only the fundamental spots are split and not the COO superlattice spots [see Fig. 5(b)]. This clearly indicates that the observed split basically arise from superimposition of zone patterns of COO1 and COO2 phases taken along zones equivalent to [010] zone of *Pnma*. The reflections due to COO2 can be differentiated from that of the COO1 with the help of COO superlattice reflections. Arrows in Fig. 5(b) indicate these. Figure 5(c) shows a schematic of the simulation of the observed pattern in Fig. 5(a). It can be noticed that the marked spots of COO2 are diagonally away along $[\bar{1}01]$. This is due to contraction of the direct lattice along $[\bar{1}01]$. This is discussed in details in the following.

The COO2 phase was observed in various other grains as well. Figure 6(a) shows an electron micrograph of a grain showing coexistence. The SAD pattern from domain marked "A" of this grain, taken along the $[0\bar{1}2]$ zone of the *Pnma*, is shown in Fig. 6(b). Figure 6(c) shows the simulated SAD pattern corresponding to the coexistence. Similarly Fig. 7 shows (a) electron micrograph and (b) SAD pattern taken along [101]. The SAD in Fig. 7(b) shows splitting of spots arising from twin domains. The consecutive twin bands ba-

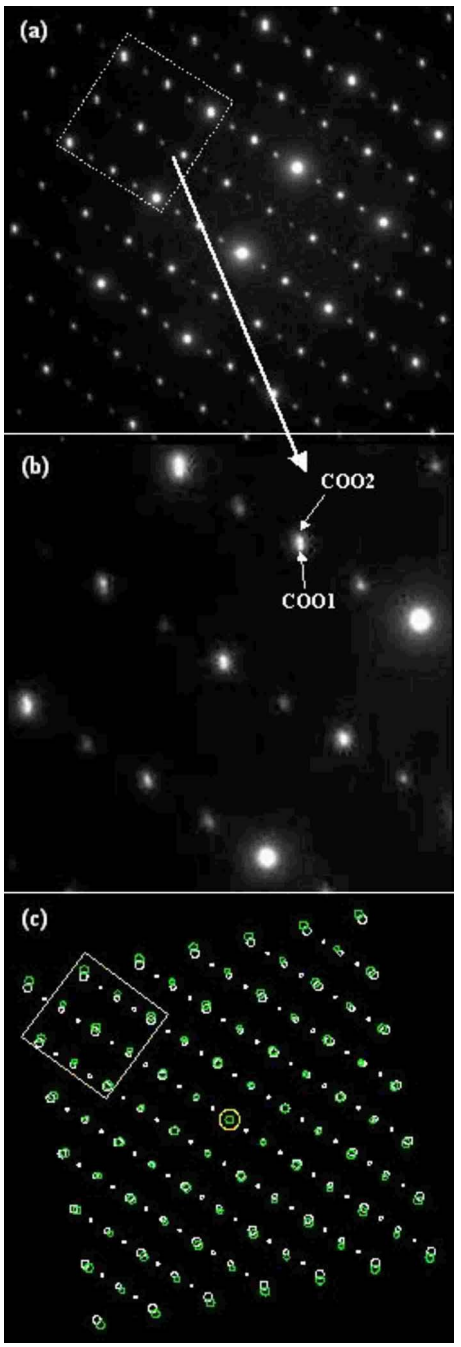

FIG. 5. (Color online) (a) [010] zone SAD pattern from the common region of COO1 and COO2. (b) An expanded portion highlighting the splitting of the spots. The split spots due to COO1 and COO2 are indicated by arrows. (c) Simulated pattern corresponding to SAD in (a). Diffraction spots of COO2 (green circles) are diagonally distorted along [−101] due to apical compression.

sically correspond to the charge-orbital ordered phases, COO1 and COO2.

The SAD in Fig. 6(b) reveals the presence of two COO phases having superlattice modulations in different directions. The superlattice spots have been indicated by white and black arrows. The superlattice spots indicated by white arrows are along [100] of the *Pnma* and belong to the COO1 phase, whereas the one indicated by black arrows are along

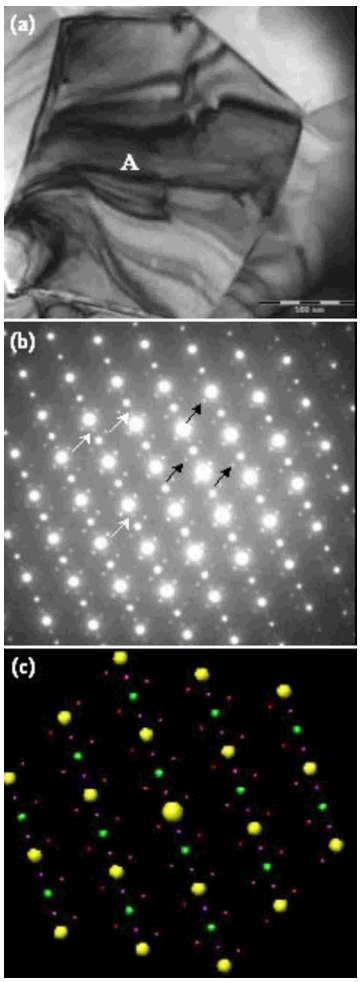

FIG. 6. (Color online) (a) Electron micrograph of a grain showing COO coexistence at 96 K. (b) [210] zone SAD pattern taken at 96 K from region A having COO coexistence. The presence of two types of superlattice modulations can be seen. Those with usual (1/2,0,0) type vector are indicated by white arrows and the other ones with (1/4,1/2,1/4) type vector are indicated by black arrows. The simulated composite diffraction pattern based on the orbital flip model has been shown in (c)

[121] of the *Pnma* and hence belong to the other phase COO2. These were identified to be arising from region marked A in the micrograph shown in Fig. 6(a). It can be noticed that the appearing superlattice spots have the same basic modulation vector as that of the parent COO1 but along [121]. The superlattice modulation vector of COO2 has identical ~2° tilt about the corresponding fundamental spots as observed for COO1 phase. These observed facts indicate that the acquired phase is also a COO phase but with a different modulation direction. The modulation direction for this COO phase is [121] of the basic *Pnma* with modulation vector (1/4,1/2,1/4). The SAD in Fig. 6(b) shows that, whatever may be the ordering direction with respect to the *Pnma*, it is always a [110] type direction of the perovskite. Thus, if we look at charge orbital in a general perspective, the COO2 phase will correspond to flipping of orbital ordering direction from [101] to $[1\bar{1}0]$ of the perovskite. We have termed this charge-orbital phase as COO2. As a result of this

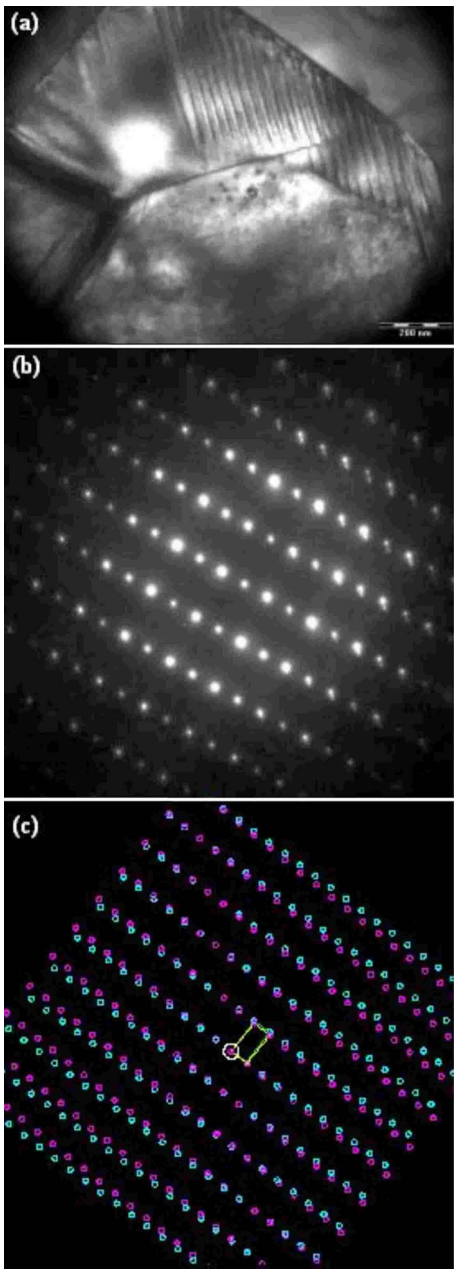

FIG. 7. (Color online) (a) Electron micrograph of a grain showing [101] oriented twin domains corresponding to COO1 and COO2 phases coexisting at 96 K. (b) [101] zone SAD pattern taken including the two types of twins at 96 K. The split spots due to COO1 and COO2 phases can be clearly seen. The simulated composite diffraction pattern calculated based on the changed apical compression is shown in (c)

flip transition, the charge-orbital ordering vector will change from (1/2,0,0) to (1/4,1/2,1/4) of *Pnma*. During this transformation the reflections corresponding to parent structure (the *Pnma*) remain nearly intact, indicating that the relative atomic positions remain nearly unchanged. Based on above analysis we could model the three-dimensional (3D) reciprocal lattice for COO2 phase. Reciprocal-lattice nets corresponding to COO1 and COO2 phases are shown in Fig. 8(a) and 8(b), respectively. A comparison of basic reciprocal unit cells of the basic perovskite, the *Pnma*, the COO1, and

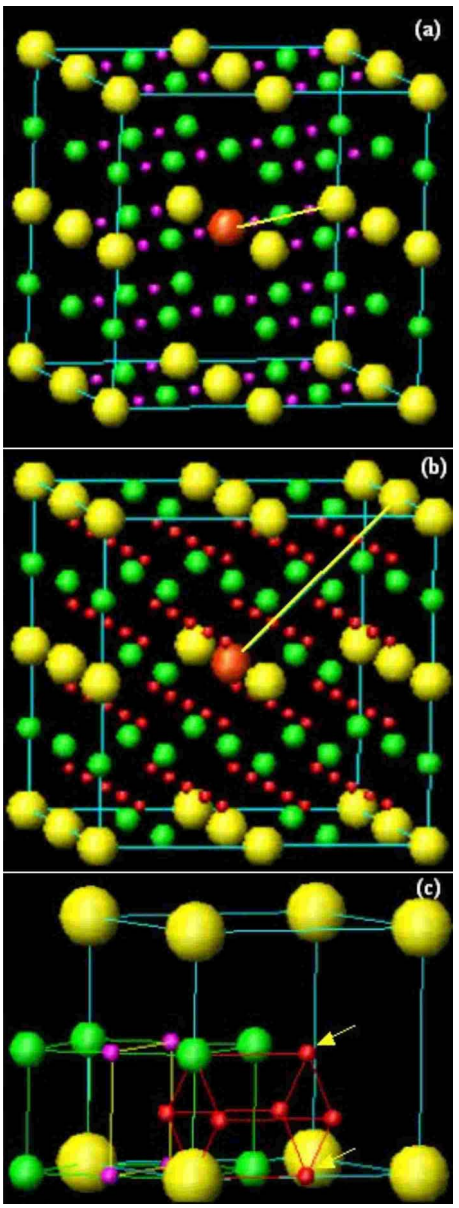

FIG. 8. (Color online) A finite portion of the reciprocal-lattice nets for (a) COO1 and (b) COO2 phases. These have been constructed based on the analysis of experimentally observed electron-diffraction patterns. (c) A comparative presentation of reciprocal-lattice unit cells for basic perovskite (yellow), *Pnma* (green), COO1 (magenta), and COO2 phases (red). The colors in the above diagrams represent different stages of ordering. Yellow is for the starting basic perovskite, the green ones appear when cubic perovskite orders to *Pnma*, the magenta ones appear when *Pnma* orders to COO1, and the red ones appear when *Pnma* orders to COO2 phases. The ordering directions for COO1 and COO2 are indicated by yellow lines.

COO2 phases, is also presented in Fig. 8(c). While constructing the reciprocal-lattice net for COO2 phase, the invisible reflections have been shown extinct. But in Fig. 8(c) the reciprocal-lattice points, which should actually be extinct, are also shown for the sake of clear visualization of the basic reciprocal cell for COO2 phase. Arrows mark these points.

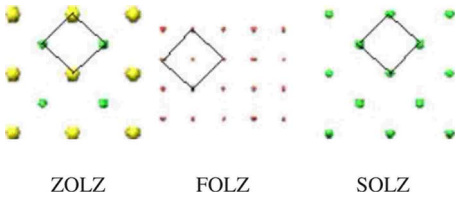

FIG. 9. (Color online) ZOLZ and HOLZ layers derived from the reciprocal-lattice net of COO2 phase. These patterns match with the enlarged view of the experimentally observed patterns shown in Fig. 2(d).

During *Pnma* to COO1 transition in a manganite, the unit-cell parameter changes from $\sqrt{2}a_p \times \sqrt{2}a_p \times 2a_p$ to $2\sqrt{2}a_p \times \sqrt{2}a_p \times 2a_p$, where a_p is the pseudoperovskite cell parameter. Keeping in view the comparison of reciprocal-lattice unit cells, as shown in Fig. 8(c), the cell parameter of COO2 phase will be $2\sqrt{2}a_p \times 2\sqrt{2}a_p \times 2a_p$.Using the reciprocal-lattice net for COO2, as shown in Fig. 8(a), we could successfully simulate the SAD and CBED patterns observed for COO2 phase. These are shown in Figs. 6(c) and 9. Figure 9 shows simulated ZOLZ and HOLZ layers observed in the CBED pattern shown in Fig. 2(d). Comparison of the unit cells, as indicated by squares in ZOLZ, FOLZ, and SOLZ reciprocal layers, do show an extra spot in the center of FOLZ layer's unit cells. This is what has experimentally been observed in Fig. 2(d). Occurrence of COO with modulation vector (1/4,1/2,1/4) has been reported by Asaka *et al.*[23] The difference between the two observations is that we observed (1/4,1/2,1/4) modulation occurring as a result of transition from (1/2,0,0) type modulation whereas Asaka *et al.*[23] have found it appearing simultaneously with (1/2,0,0) as a composite modulation in a domain of $Pr_{5/8}Ca_{3/8}MnO_3$, which has excess e_g orbitals.

The phase transition from COO1 to COO2 is a result of flipping of e_g orbitals from one ordered configuration $d_{3x^2-r^2}/d_{3y^2-r^2}$ to another ordered configuration $d_{3x^2-r^2}/d_{3z^2-r^2}$. In COO1 phase the $d_{3x^2-r^2}/d_{3y^2-r^2}$ orbitals are ordered in (010) plane of the *Pnma* but in COO2 the $d_{3x^2-r^2}/d_{3z^2-r^2}$ orbitals are ordered in $(\bar{1}01)$ plane. Structural models for COO2 and COO1 are shown in Figs. 10(a) and 10(b). Figures 10(c) and 10(d) show comparison of orientations of the orbitals in (010) and $(\bar{1}01)$ planes, respectively. From the observed SAD results, it appears that the tilt of MnO_6 octahedra remains nearly unaffected during this orbital flip transition. In a disordered state of e_g orbitals, the octahedral coordination of oxygen about manganese is undistorted. The six Mn-O bonds are all equal. In COO1 type ordered state e_g orbitals get arranged in zigzag pattern in (010) plane (the *a*-*c* plane). Due to this the two Mn-O(1) distances along the *b* axis get *apically compressed*[21] than the other four Mn-O(2) distances in the *a*-*c* plane, implying a *reverse* Jahn-Teller distortion.[24] During flip transition the e_g orbitals, which were initially arranged in (010) set of planes, now get reoriented and arranged in $(\bar{1}01)$ set of planes causing *compression* of Mn-O bonds along $[\bar{1}01]$. Now since the *compression* is shifted from [010] to a direction normal to [010], the *b* parameter of the *Pnma* phase should relatively

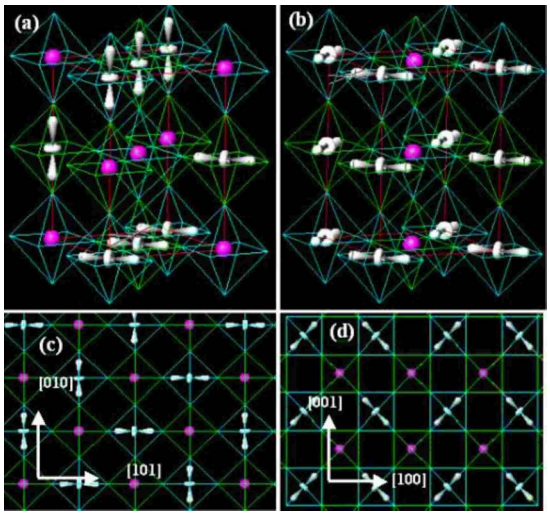

FIG. 10. (Color online) (a) Structural model of COO2 phase. The orientations and positions of e_g orbitals of Mn^{+3} (dumbbells) together with Mn^{+4} (spheres) have been shown with respect to the *Pnma* unit cell (red). The antiphase tilted MnO_6 octahedra are shown in green and blue. Comparison of e_g-orbital flips of COO2 phase with respect to the COO1 can be seen in the structural model of COO1 shown in (b). (c) and (d) show the planes of orbital ordering in COO2 and COO1 phases, respectively.

expand in COO2 as compared to COO1. The *compression* along $[\bar{1}01]$ will distort the orthorhombic *Pnma* lattice into a monoclinic lattice. This is what has actually been observed in the SAD patterns shown in Figs. 5 and 7(b). We could confirm the orthorhombic to monoclinic distortion in COO2 phase by measuring the angle between a^* and c^* to be $88 \pm 1°$ from the SAD pattern shown in Fig. 2(b). By considering the monoclinic distortion, we successfully simulated [Fig. 5(c)] the splitting of diffraction spots in the SAD patterns taken from coexisting regions [Figs. 5(a) and 5(b)]. The expansion of *b* axis is fully accounted by the simulation [Fig. 7(c)] of SAD pattern in Fig. 7(b). Thus the analysis of the observed SAD patterns is fully consistent with the flipping of e_g orbitals, as discussed above. The occurrence of in-plane orbital flip transition, i.e., from $d_{3x^2-r^2}/d_{3y^2-r^2}$ to $d_{3y^2-r^2}/d_{3x^2-r^2}$, has been observed earlier[25] for double layer manganite $LaSrMnO_7$. The presently observed orbital flipping is thus different in nature. In order to check the presence of any chemical inhomogeneity, the regions corresponding to COO1 and COO2 were very carefully examined through energy dispersive x-ray spectroscopy (EDS) analysis, and were found to be of same chemical composition. Interesting and the most important point to note is that the features shown in the micrographs of Fig. 4 were found to exactly reproduce during repeated heating-cooling cycles between room temperature to 96 K.

The occurrence of hysteresis, as shown in Fig. 3, indicates as if the observed phase transition of COO1 into COO2 is a temperature driven first-order phase transition. Had it been truly a temperature driven first-order transition, then due to random nucleation and growth, the microstructure of COO2 phase should have shown variation in its spatial position after each thermal cycle and at 96 K; it should have been

totally transformed to COO2 phase. But on the contrary, the microstructure was found to exactly reproduce during repeated heating-cooling cycles and COO1 phase was found to coexist with the COO2 phase even at 96 K. This indicates that COO2 phase appears as a result of variation in some other physical parameter of the sample than its temperature. Keeping in view the absence of chemical inhomogeneity in the sample, the other possible parameter appears to be strain field, which is related to the lattice degrees of freedom.

In orthorhombic manganites, which have anisotropic thermal-expansion coefficients along [010] and [100], presence of local strain in a densely sintered pellet of randomly oriented grains is very much likely. It has been found[3,26] that when an orthorhombic (*Pnma*) manganite is cooled, its **b** axis contracts while **a** and **c** axes expand. This behavior becomes drastic[26] around the COO transition temperature, at which the contraction and expansion rates are the maximum. Now in a densely sintered pellet, where grains are randomly oriented, the interface between grains will in general contain some component of expansion due to one grain and some component of contraction due to the other. Therefore a local strain will build up during cooling. At a given temperature maximum local strain at an interface will be in a situation when it is made up of planes such that [010], and [100]/[001] are parallel. When orientations of two grains are the same, the local strain at their interface will be zero. Thus, due to random orientation of grains, a pellet sample will have a distribution of such local strains in it. There will be situations in which grains may effectively be clamped under compressive or tensile stress. Growth of triangular patch of twin domains starting from the grain boundary strongly supports this (see Fig. 4). In a scattering experiment such strain will show up as large asymmetry and/or broadening of the diffraction peaks. Such strain will be maximum below COO but due to lattice mismatch, it will have nonzero value even at room temperature. Since *Pnma* phase appears as a result of solid-solid transformation at temperatures much higher than RT, where interfaces are already rigid, such a local strain will build up even at RT while cooling the pellet after sintering. It should be noted that such local strain will be purely due to interfaces formed by rigidly joined grains. Therefore when these grains are separated from each other, the local strain and its effect on the structural and physical properties of the sample will also disappear.

Figure 11 depicts superimposed XRD profiles of the pellet and powder samples of $Pr_{0.5}Ca_{0.5}MnO_3$. Magnified view of some of the important regions is given in the inset. The large asymmetry manifested by the hump about the intense peak can be clearly seen. The hump has completely disappeared in the XRD profile of the corresponding powder sample. In pellet, the humplike broad peaks further grow at low temperatures. Presence of extra peaks corresponding to the coexisting monoclinically distorted lattice, which is basically the COO2 phase, is shown in the fitted profile in Fig. 12. In the case of powder sample, we could not see any signature of COO2 phase at low temperatures. This indicates that monoclinically distorted phase, i.e., the COO2 phase, is present only in the pellet sample and not in the corresponding powder sample. This directly implies that the observed orbital flip transition is not an intrinsic property of $Pr_{0.5}Ca_{0.5}MnO_3$,

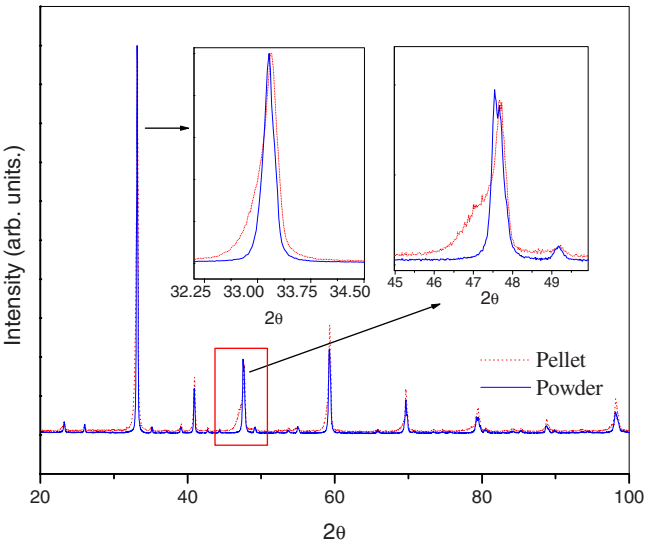

FIG. 11. (Color online) Room-temperature XRD pattern for pellet (red dotted) and the corresponding powder (blue solid line) samples of $Pr_{0.5}Ca_{0.5}MnO_3$. The large asymmetry in the XRD of pellet sample, arising due to the presence of the humplike feature, can be clearly seen in the insets.

rather, it appears only in its pellet version. As discussed above, the strain gets released on separating the grains from each other by grinding the pellet and hence the corresponding orbital flip transition also vanishes. From low-temperature XRD data, the volume fractions of conventional and the acquired COO phases (COO2) in the pellet sample of $Pr_{0.5}Ca_{0.5}MnO_3$ is estimated to be ~55% and 45%, respectively. It should be noted that in such cases, on thinning pellet samples to a thickness lower than the average grain

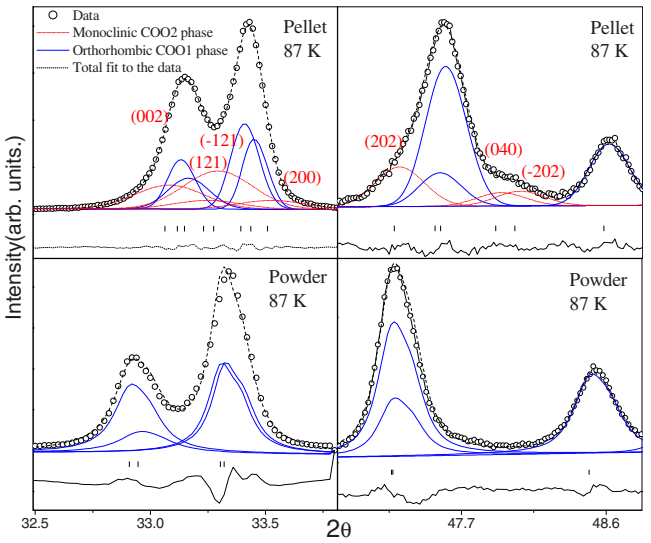

FIG. 12. (Color online) Profile fitting of XRD peaks from the pellet and the corresponding powder samples of $Pr_{0.5}Ca_{0.5}MnO_3$. For pellet's XRD the profile could be fitted properly (dashed line) only when fitting was done including both orthorhombic (COO1) and monoclinic (COO2) phases. The XRD peaks (red dotted) of the COO2 phase are indexed. The peaks in blue (solid line) correspond to COO1 phase.

size, the local strain will largely be released due to decreased interface area and hence the number of grains undergoing orbital flip transition will also decrease. Therefore the estimate of percentage of grains showing orbital flip transition, which was made based on TEM observation, is much lower than that of the XRD data.

Looking at the differences in the features of COO superlattice spots, it so appears that grains having certain minimum strain at RT do not undergo conventional COO. As described above, on lowering the sample temperature, the local strain on that grain starts increasing. To accommodate this strain, the COO direction tilts up to certain extent, as shown in the inset of Fig. 3. The observed tilting of the direction of COO clearly indicates that charge ordering do have certain degree of itinerancy, i.e., it has characters of CDW. This feature is in accordance with the recently reported[12] sliding of CDW on application of electric field. With decreasing temperature the strain below ~145 K becomes large enough for the existing ordered orbital arrangement to further accommodate in (010) plane just by tilting itself about [010] and hence it flips to another possible lower energy configuration. It should be noted that d_{3x^2} type e_g orbitals have three possible orientations. Depending on the physical constraints, they may align themselves parallel to any of the three unit-cell directions x, y, and z of the basic perovskite lattice. The hysteresis shown in Fig. 3 is actually a response against strain, which builds up only when the sample temperature is lowered below T_{co} and hence the flipping will not be seen at RT. Appearance of only COO1 phase in powder sample of PCMO at low temperatures perhaps may appear to indicate that the observed COO1 to COO2 phase transition is not an intrinsic property of PCMO but it is misleading. The observed phase transition is very much an intrinsic behavior of PCMO. For this, one will have to consider a more general phase diagram of PCMO: a 3D phase diagram with three axes *composition*, *temperature*, and *strain* (effectively a uniaxial pressure).

In-plane flipping of e_g orbitals in double layer manganite $LaSrMn_2O_7$ has been reported[25] to cause interesting changes in its optical properties and therefore it has device potential. It is quite likely that the strain dependence of the orbital flipping, as observed in the present investigation, may also be exploited for some similar switchable device.

IV. CONCLUSION

Based on the above described low-temperature transmission electron microscopy and x-ray diffraction studies, we conclude that charge-orbital ordering in $Pr_{0.5}Ca_{0.5}MnO_3$ is very rugged and undergoes a first-order orbital flip transition of e_g orbitals from $d_{3x^2-r^2}/d_{3y^2-r^2}$ to $d_{3x^2-r^2}/d_{3z^2-r^2}$ configuration, which results in a superlattice ordering along (1/4,1/2,1/4) direction of the *Pnma* phase. This COO phase (COO2) coexists with the conventional COO phase (COO1). Low-temperature XRD studies on pellet and powder samples show that the COO phase occurs only in pellet sample and not in the powder sample. The occurrence of reproducible features in TEM micrographs observed during heating and cooling cycles indicate that the COO2 phase appears due to local lattice strain in the pellet sample arising as a result of anisotropic thermal expansion in manganites.

ACKNOWLEDGMENTS

Authors gratefully thank P. Chaddah, the Director, and A. Gupta, the Center-Director of UGC-DAE-CSR Indore, for their interest in the work and helpful discussions. Thanks are also due to Archna Sagdeo, Raja Ramanna Centre for Advanced Technology, Indore for critical reading of the manuscript and suggesting possible corrections. One of us (A.V.N.) thanks Indian National Science Academy for financial support to pursue this work.

[1] J. C. Loudon, N. D. Mathur, and P. A. Midgley, Nature (London) **420**, 797 (2002).
[2] D. D. Sarma, D. Topwal, U. Manju, S. R. Krishnakumar, M. Bertolo, S. La Rosa, G. Cautero, T. Y. Koo, P. A. Sharma, S. W. Cheong, and A. Fujimori, Phys. Rev. Lett. **93**, 097202 (2004).
[3] P. R. Sagdeo, Shahid Anwar, and N. P. Lalla, Phys. Rev. B **74**, 214118 (2006).
[4] M. Pissas, I. Margiolaki, K. Prassides, and E. Suard, Phys. Rev. B **72**, 064426 (2005).
[5] Y. Tokura and N. Nagaosa, Science **288**, 462 (2000).
[6] A Moreo, S. Yunoki, and E. Dagotto, Science **283**, 2034 (1999).
[7] E. Dagotto, T. Hotta, and A. Moreo, Phys. Rep. **344**, 1 (2001).
[8] E. Dagotto, *Nanoscale Phase Separation and Colossal Magnetoresistance*, Springer Series in Solid State Sciences Vol. 136 (Springer, New York, 2203).
[9] J. Burgy, M. Mayr, V. Martin-Mayor, A. Moreo, and E. Dagotto, Phys. Rev. Lett. **87**, 277202 (2001).
[10] V. B. Shenoy, T. Gupta, H. R. Krishnamurthy, and T. V. Ramakrishnan, Phys. Rev. Lett. **98**, 097201 (2007).
[11] K. H. Ahn, T. Lookman, and A. R. Bishop, Nature (London) **428**, 401 (2004).
[12] S. Cox, J. Singleton, R. D. McDonald, A. Migliori, and P. B. Littlewood, Nature Mater. **7**, 25 (2008).
[13] P. W. Kolb, D. B. Romero, H. D. Drew, Y. Moritomo, A. B. Souchkov, and S. B. Ogale, Phys. Rev. B **70**, 224415 (2004).
[14] M. A. Fradkin, J. Phys.: Condens. Matter **9**, 7925 (1997).
[15] Y. Tomioka, A. Asamitsu, Y. Moritomo, and Y. Tokura, J. Phys. Soc. Jpn. **64**, 3626 (1995).
[16] A. M. L. Lopes, J. P. Araújo, V. S. Amaral, J. G. Correia, Y. Tomioka, and Y. Tokura, Phys. Rev. Lett. **100**, 155702 (2008).
[17] A. Banerjee, K. Mukherjee, K. Kumar, and P. Chaddah, Phys. Rev. B **74**, 224445 (2006).
[18] Z. Jirák, S. Krupička, Z. Šimša, M. Dlouhá, and S. Vratislav, J. Magn. Magn. Mater. **53**, 153 (1985).
[19] S. Shimomura, T. Tonegawa, K. Tajima, N. Wakabayashi, N. Ikeda, T. Shobu, Y. Noda, Y. Tomioka, and Y. Tokura, Phys. Rev. B **62**, 3875 (2000).
[20] C. H. Chen and S.-W. Cheong, Phys. Rev. Lett. **76**, 4042 (1996).

[21] P. G. Radaelli, D. E. Cox, M. Marezio, and S.-W. Cheong, Phys. Rev. B **55**, 3015 (1997).
[22] P. R. Sagdeo, Shahid Anwar, and N. P. Lalla, Powder Diffr. **21**, 40 (2006).
[23] T. Asaka, S. Yamada, S. Tsutsumi, C. Tsuruta, K. Kimioto, T. Arima, and Y. Matsui, Phys. Rev. Lett. **88**, 097201 (2002).
[24] P. G. Radaelli, D. E. Cox, L. Capogna, S.-W. Cheong, and M. Marezio, Phys. Rev. B **59**, 14440 (1999).
[25] Y. Tokunaga, T. Lottermoser, Y. S. Lee, R. Kumai, M. Uchida, T. Arima, and Y. Tokura, Nature Mater. **5**, 937 (2006).
[26] M. R. Ibarra, J. M. De Teresa, J. Blasco, P. A. Algarabel, C. Marquina, J. García, and J. Stankiewicz, Phys. Rev. B **56**, 8252 (1997).